Polymer 55 (2014) 3168–3177

Contents lists available at ScienceDirect

Polymer

journal homepage: www.elsevier.com/locate/polymer

Probing conformational transitions of polymer chains by microrheology

Chih-Hsing Huang [a], Yen-Ching Li [a], Yi-Qi Yeh [b], U-Ser Jeng [b], Hsien-Hung Wei [a,*], Jeng-Shiung Jan [a,*]

[a] Department of Chemical Engineering, National Cheng Kung University, Tainan 701, Taiwan
[b] National Synchrotron Radiation Research Center, Hsinchu 300, Taiwan

ARTICLE INFO

Article history:
Received 20 December 2013
Received in revised form
29 April 2014
Accepted 1 May 2014
Available online 10 May 2014

Keywords:
Coil–globule transition
Microrheology
Poly-2-vinylpyridine

ABSTRACT

We report the first quantitative demonstration of the use of particle tracking microrheology (PTμR) in probing the pH-induced coil–globule transition (CGT) of poly-2-vinylpyridine (P2VP). The calculated radii R of the P2VP coils and globules are found to vary with molecular weight M respectively according to: $R \propto M^{0.592 \pm 0.006}$ and $R \propto M^{0.339 \pm 0.010}$, in excellent agreement with the classical Flory–de Gennes theory. The sphere-like small-angle X-ray scattering spectrum and the sharp rise in pyrene emission suggest that the observed CGT is likely triggered by drastic changes in the chain's hydrophobicity, sensitive to the degree of protonation near the coil–globule transition point. A more in-depth theoretical analysis further reveals that the phenomenon strongly depends on interplays between excluded-volume, electrostatic, and hydrophobic interactions at the subunit level of a P2VP chain. This new application of PTμR could have potential uses in exploring the physics of a variety of polymer systems at the nano/molecular scales.

1. Introduction

It is well known that a polymer chain can change its conformation due to molecular interactions between its own segments and/or its affinity to the surrounding solvent. Such a change is manifested not only by a chain's global appearance through its size or shape, but also by the detailed microstructure characterized by many internal length scales (e.g. persistence length, intersegment spacing, correlation length, etc.). In a good solvent where the chain segments tend to self avoid each other due to excluded volume effects, the chain behaves like a swollen coil. In contrast, in a poor solvent, because the chain segments dislike the solvent, it is more favorable for the chain to form a compact globule by minimizing its contact with solvent molecules. When the solvent quality turns from good to poor (via changing temperature, composition, pH, etc.), the chain might undergo an abrupt conformational change from the coiled state to the globular state. This is the well-known coil–globule transition (CGT), which has been studied extensively in the context of polymer physics [1–3]. A similar phase transition can also occur to polymer gels, displaying a discontinuous volume change or the so-called volume phase transition [4]. In either case, if looking at the microstructure of a polymer solution over the chain/blob scale, the density inside a polymer coil/blob can exhibit an abrupt decrease when chains turn from the expanded state into the more compact state. Much like the vapor–liquid phase transition, such a chain expansion/compaction process represents a transition from a loose state to a much dense state for chain segments when their interactions turn from repulsion into attraction. Studying such a transition is essential because it provides an understanding of how chain segments interact and hence guidance for a precise control of the swollenness/compactness of a polymer chain.

Aside from its fundamental importance, conformational transition also plays important roles in biological applications and chemical processing. For instance, DNA can be condensed into a more compact structure, which can be used for gene delivery [5,6]. In terms of chemical processing, if one wishes to functionalize polymer chains, it is more desirable to have them dissolved in a good solvent so that reactants can readily penetrate into the chains for facilitating their binding. For polymer adsorption, on the other hand, it might better work in a poor solvent, since polymer chains would prefer to stay on a lower-energy substrate to reduce their contacts with solvent molecules [7].

* Corresponding authors.
E-mail addresses: hhwei@mail.ncku.edu.tw (H.-H. Wei), jsjan@mail.ncku.edu.tw, jamesjan112@hotmail.com (J.-S. Jan).

http://dx.doi.org/10.1016/j.polymer.2014.05.001
0032-3861/

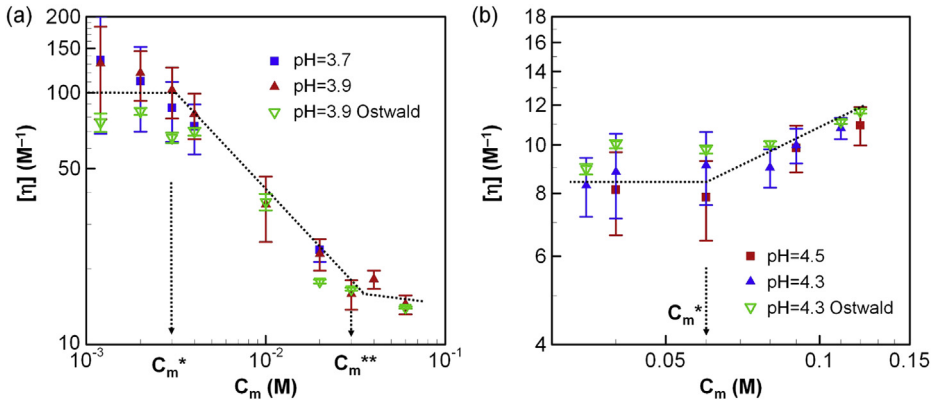

Fig. 1. Plot of intrinsic viscosity $[\eta]$ against monomer concentration C_m for **2-VP1500** solution at (a) pH < 4 and (b) pH > 4. The PTμR data (blue and red symbols) show good agreement with those measured by the Ostwald viscometer (green symbols). For each case, the value of C_m^* is roughly determined at the point where $[\eta]$ starts to vary with C_m. The respective C_m^* values for (a) and (b) are about 0.003 and 0.06 M. C_m^{**} likely marks the transition point from the unentangled regime to the entangled regime. (For interpretation of the references to color in this figure legend, the reader is referred to the web version of this article.)

Several techniques have been employed to probe conformational changes of polymer chains, including dynamic light scattering (DLS) [3,8], fluorescence correlation spectroscopy (FCS) [9,10], atomic force microscopy (AFM) [11–14], and small angle neutron scattering (SANS) [15,16]. Rheological measurements have also been suggested as an alternative to reveal how polymer chains change their hydrodynamic volumes in connection to the viscosity of a polymer solution [17,18]. However, using conventional rheology to infer polymer sizes at equilibrium might be inaccurate because the measurements have to be made under hydrodynamic flows, which could lead to deformations of polymer chains. In contrast, in microrheology, one can make use of probe particles to directly probe the microstructure of a sample solution by measuring solution viscosity without external forcing [19–21]. Compared to conventional rheology, this approach requires only microliter-sized samples. And more importantly, it is relatively sensitive to low-viscosity samples and easy to implement. Together with the ability to implement fast acquisition for particle trajectories, this passive approach can readily generate rheological phase diagrams for macromolecules [22]. It has also been reported that microrheology can be employed to quantify how proteins change their sizes due to folding and unfolding [23], showing potential in probing conformational changes of polymer chains. Along this line, this idea has been further extended to study the behavior of polyelectrolytes in the presence of multivalent salts [24], demonstrating that it is capable of inferring the unusual chain collapse and reexpansion phenomena reported in simulations [25]. In addition, microrheology has emerged as a powerful approach for elucidating viscoelastic properties of polymer monolayers [26] or complex fluids such as entangled polymer solutions, interconnected polymer networks, or gels [20,27–31].

Based on these previous studies, passive microrheology seems to be a feasible approach to study conformational changes of polymer chains. Compared to other techniques such as DLS and FCS, the sample preparation of this approach is relatively simple because it is not sensitive to impurities nor requires additional luminous labels. It also has potential uses in studying how polymer chains deform under external stimuli, offering an enabling tool for characterizing their behaviors under various conditions. While there are many benefits for microrheology, existing studies, even for the simplest situation without external forcing, mainly look at viscosity changes of sample solutions to infer possible conformational changes thereof qualitatively. So the question is: can microrheology be used to perform more quantitative studies for directly pointing toward the natures of a polymer chain at the single molecule level? To our best knowledge, this technique has not been rigorously tested for such a purpose.

In this work, we demonstrate that particle tracking microrheology (PTμR) is indeed capable of accurately capturing how a polymer chain changes its size and hence of quantifying its conformational transition. Here we choose poly-2-vinylpyridine (P2VP) as our model polymer to look at its conformational transition due to pH changes. As will be demonstrated below, we employ PTμR to measure the viscosities of P2VP solutions and extract the sizes of P2VP coils and globules from the PTμR data. By doing so, we not only recover the sharp conformational transition reported previously [10] (see Fig. 2), but also are able to establish scaling laws for how the coil and globule sizes of P2VP vary with molecular weight (see Fig. 3). More importantly, we find the scaling laws in excellent agreement with those predicted by the classical Flory–de Gennes theory [2], justifying the use of PTμR in probing conformational changes of polymer chains. To provide more insights into how P2VP changes its structure due to pH change and how the coil–globule transition occurs, SAXS and pyrene studies will also be carried out (see Figs. 4 and 5). A more in-depth theoretical analysis

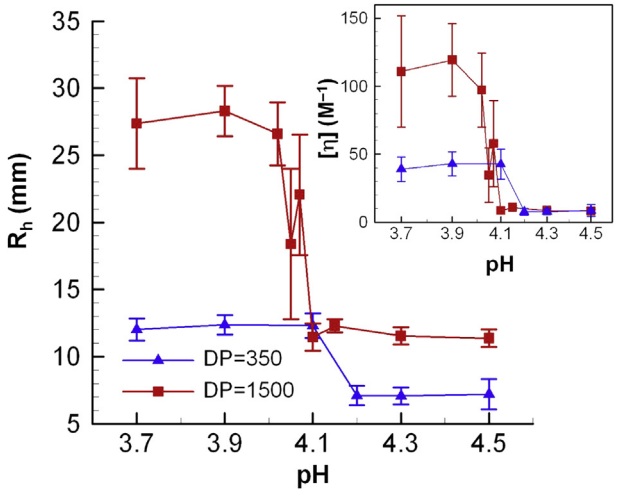

Fig. 2. Plot of hydrodynamic radius R_h against pH for **2-VP350** and **2-VP1500** solutions. An occurrence of chain collapse is clearly indicated by significant drop of R_h at around the transition point pH ≈ 4.1, as also seen in the inset for the corresponding decrease in intrinsic viscosity $[\eta]$. At pH ≦ 4.1, the monomer concentrations for **2-VP350** and **2-VP1500** are 0.002 and 0.006 M, respectively. At pH > 4.1, the monomer concentration for both samples is 0.02 M.

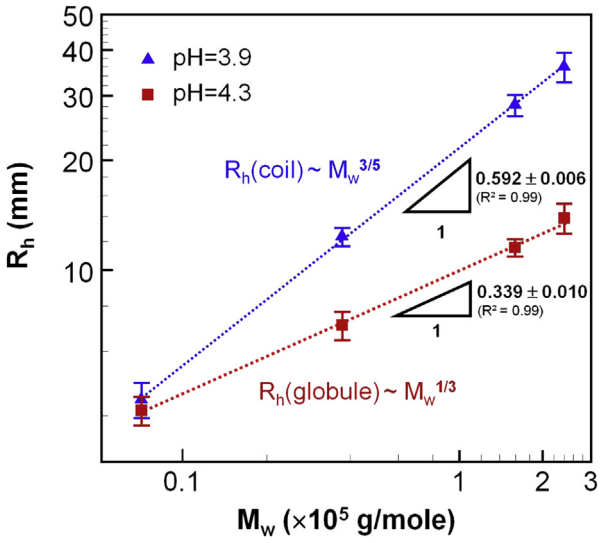

Fig. 3. Distinct dependences of hydrodynamic radius R_h on molecular weight M_w at pH = 3.9 and pH = 4.3. At pH = 3.9 below the transition point pH ≈ 4.1, we find $R_h \propto M_w^{0.592\pm0.006}$, in excellent agreement with $R_h \propto M_w^{3/5}$ at the swollen coil state according to the classical Flory–de Gennes theory. In fact, this result much better agree with $R_h \propto M_w^{0.588}$ obtained by the renormalization group theory (see Ref. [26]). At pH = 4.3 beyond the transition point, the relationship turns to $R_h \propto M_w^{0.339\pm0.010}$, which also agrees with $R_h \propto M_w^{1/3}$ at the compact globular state predicted by the theory. At pH = 3.9, the monomer concentrations for **2-VP70**, **2-VP350**, **2-VP1500**, and **2-VP2400** are 0.02, 0.006, 0.002, and 0.0014 M, respectively. At pH = 4.3, the monomer concentration for all samples is 0.02 M.

(see Section 4.6) will further reveal how intrachain interactions play roles in the observed conformational transition.

2. Background

2.1. Coil–globule transition (CGT)

Prior to probing CGT using PTμR, it is necessary to review how a polymer chain changes its conformation, which is described by the classical Flory–de Gennes theory [2]. According to this theory, the equilibrium coil size R can be determined by minimization of the free energy of the chain F. This energy consists of the entropic energy, the two-body self energy between monomers (characterized by the second virial coefficient v_2 that can be either >0 or <0), and the three-body self energy (characterized by the third virial coefficient $v_3 > 0$) [2]:

$$\frac{F}{k_BT} = 3\left(\frac{R^2}{2b^2N} - \ln\frac{R}{bN^{1/2}}\right) + \frac{v_2N^2}{R^3} + \frac{v_3N^3}{R^6}. \quad (1)$$

Here b is the Kuhn length and N is the number of Kuhn segments. The latter is proportional to molecular weight M_w. Returning to Eq. (1), we further include the ln R term in the entropic energy to account for entropic mixing. This ensures the chain to maintain ideal $R = bN^{1/2}$ at the theta point $v_2 = 0$. In good solvents where the intrachain interactions are dominated by excluded volume with $v_2 > 0$, the chain tends to be swollen by solvent molecules. Balancing the v_2 term with the entropic term gives the well-known Flory's scale:

$$R \sim \left(v_2b^2\right)^{1/5}N^{3/5} \propto M_w^{3/5} \quad (2)$$

In poor solvents, however, the chain segments prefer to stay together for reducing their contacts with the solvent. Specifically, the attractive intrachain interactions with $v_2 < 0$ leads the chain to shrink in the direction of reducing the free energy at the rate of R^{-3}. But the entropic penalty due to this attraction-induced shrinkage is too great to be compensated by the chain elastic energy. So the chain has to collapse all the way to a compact globule where the three-body excluded volume repulsion of R^{-6} (with $v_3 > 0$) becomes sufficiently strong to stop the collapse. By balancing the last two terms in Eq. (1), the resulting globule size can be estimated as

$$R \sim (v_3/|v_2|)^{1/3}N^{1/3} \propto M_w^{1/3} \quad (3)$$

As Eqs. (2) and (3) have distinct dependences on M_w, we can use them to test if the calculated coil and globule sizes follow these scalings respectively and hence an occurrence of CGT.

2.2. Microrheology

Microrheology is a technique that enables to reveal the microstructure of a solution by monitoring the Brownian motion of probe particles [23,24]. Such a motion is often characterized by the mean square displacement (MSD) of added probe particles. Because the diffusivity of these particles can be described by the celebrated Stokes–Einstein equation [32], this provides a link between the MSD of probe particles (of radius a) to the viscosity η of a polymer solution:

$$\mathrm{MSD} = \left\langle \Delta\vec{x}(\tau)^2 \right\rangle \equiv \left\langle |\vec{x}(t+\tau) - \vec{x}(t)|^2 \right\rangle = \frac{dk_BT}{3\pi\eta a}\tau, \quad (4)$$

where k_BT is the thermal energy that causes the MSD of probe particles to vary linearly with the lag time τ. The dimensionality d of the trajectories is taken to be 2 under conventional microscopy.

Swelling (deswelling) of polymer chains in a solution can increase (decrease) the volume fraction $\Phi = (4\pi/3)C_mR^3/N$ of polymer chains and hence the solution viscosity η, where R is the coil size of a polymer chain, C_m the monomer concentration (which is the concentration (g/L) of the polymer in solution divided by the monomer molecular weight). Further assume that a polymer coil behaves like a hard sphere. If the solution is sufficiently dilute, the relationship between Φ and η can then be related in terms of the specific viscosity η_{sp} according to the Einstein–Batchelor equation [33]:

$$\eta_{sp} = \frac{\eta - \eta_s}{\eta} = 2.5\Phi + 7.6\Phi^2, \quad (5)$$

where η_s is the solvent viscosity in the absence of polymer chains. It turns out that it is more convenient to use the intrinsic viscosity $[\eta]$ to reflect the viscosity change due to chain swelling/deswelling:

$$[\eta] \equiv \frac{\eta - \eta_s}{C_m\eta_s} = \frac{10\pi}{3}\frac{R^3}{N}. \quad (6)$$

In deriving (6), for simplicity, we neglect the $O(\Phi^2)$ term (that accounts for hydrodynamic interactions [33]). As indicated by (6), $1/[\eta]$ is simply the monomer density inside the coil $\rho \sim N/R^3$, providing a direct link between $[\eta]$ and R. In other words, as long as η is measured from the MSD using (4), we can then determine the coil size R (more precisely, the hydrodynamic size R_h) of P2VP using (6) and monitor how it varies with pH. Notice that in the Flory–de Gennes theory described in Section 2.1, pH can change the virial coefficients that control interactions between chain segments. How the coil–globule transition occurs due to pH effects will be discussed in Section 4.6.

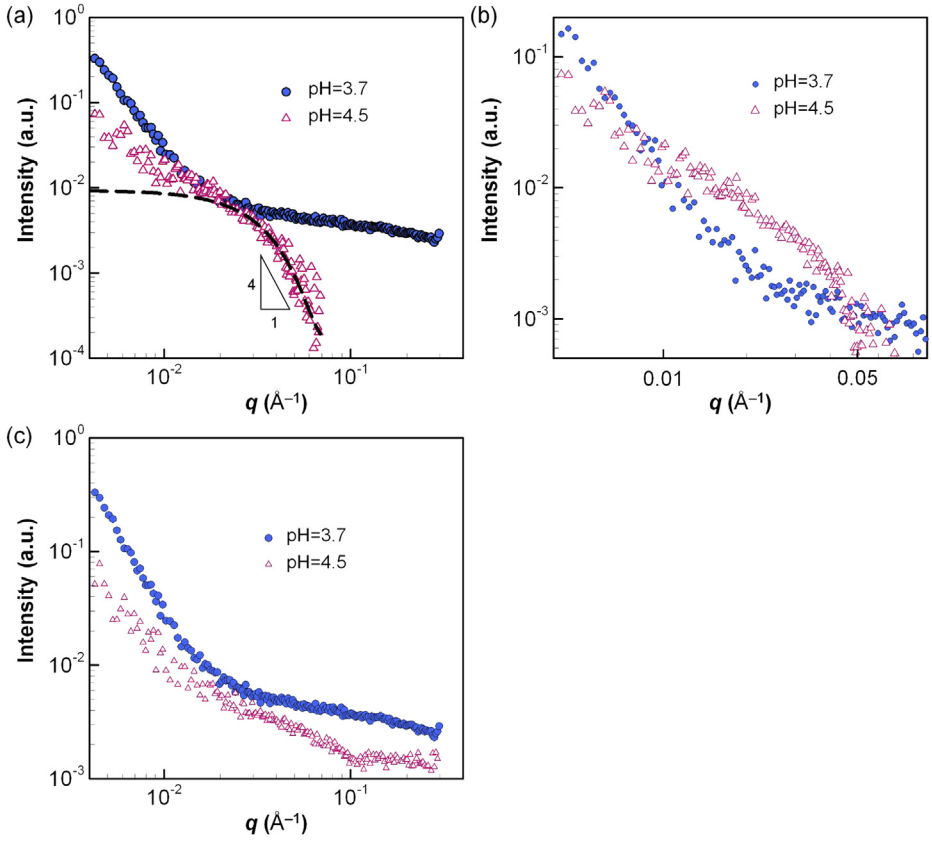

Fig. 4. SAXS spectra of P2VP chains at pH = 3.7 and pH = 4.5. They all show apparent slope changes before and after the transition point pH ≈ 4.1, suggesting conformational changes of P2VP chains. For a short chain **2-VP70** shown in (a), the Porod-like q^{-4} decay seen at pH = 4.5 indicates that the chain can exhibit a more dense and compact structure, consistent with the globular state identified in Fig. 3. (b) is the blowup view of (a) for q around 0.02 Å, showing how the SAXS intensities change with q in more detail. For a long chain **2-VP1500** shown in (c), the data at pH = 4.5 display two humps separated by a small, downward cusp at $q \approx 0.1$ Å, reminiscent of the hard-sphere signature seen in (a). At pH = 3.7, the monomer concentrations for **2-VP70** and **2-VP1500** are 0.02 and 0.006 M, respectively. At pH = 4.5, the monomer concentrations for both samples are 0.02 M.

3. Experimental section

3.1. Materials

The sodium poly(2-vinylpyridine) samples were purchased from Polysciences and Sigma–Aldrich. Four P2VP samples with different molecular weights were used: **2-VP70** (M_w = 7600, M_w/M_n = 1.36, Polysciences), **2-VP350** (M_w = 37,500, M_w/M_n = 1.07, Sigma–Aldrich), **2-VP1500** (M_w = 159,000, M_w/M_n = 1.05, Sigma–Aldrich), and **2-VP2400** (M_w = 240,000, M_w/M_n = 1.7, Polysciences). Sodium chloride (NaCl) and pyrene (98%) were purchased from Fisher Scientific and Sigma–Aldrich, respectively. All these chemicals were used without further treatment. Probe particles were taken from a 1% suspension of green fluorescent polymer microspheres of diameter 0.92 μm (Fluoro-Max™, Thermo Scientific).

3.2. Sample preparation

A P2VP solution at a desired monomer concentration (C_m) was first prepared by dissolving P2VP in an acid environment. 1 M of NaCl was added to ensure that the ionic strength of the solution does not change significantly while varying pH. It has been reported that the coil size of P2VP virtually does not change with [NaCl] when [NaCl] > 0.6 M [9]. The pH level of the solution was then adjusted using 1 M HCl or 1 M NaOH solutions. To systematically study the conformational transition of P2VP, various P2VP samples at different C_m and pH values were also prepared by following the above procedures.

3.3. Measurement of solution viscosity

To measure the viscosity of a P2VP solution using PTμR, 40 μL of the probe particles was added into 10 mL of the solution. To minimize effects of the probe particles on the viscosity measurements, we took the volume fraction of the probe particles to be $\phi_p = 4 \times 10^{-5}$. This is at least two orders of magnitude lower than the volume fraction of P2VP chains. Therefore, the increase in solution viscosity due to the addition of probe particles is not more than 0.1% of that due to the addition of P2VP. To ensure uniform dispersion of the particles, the particle–polymer solution was stirred for about 10 s, followed by sonication for about 180 s. The particle tracking experiment was conducted in a sealed polydimethylsiloxane (PDMS) microdevice (18 mm × 10 mm × 190 μm) on a glass substrate under an inverted microscope (Nikon TE-2000-U) equipped with a 640 × 480 pixel CCD camera (JVC TK-C1360B). A schematic diagram of this setup is shown in Scheme 1. The tracking was taken at 30 frames per second and recorded using specialized acquisition software (Honestech TVR). Image analysis software (IDL, Research Systems Inc.) was employed to identify the particle trajectories, tabulating the time evolution of particle positions [19,20]. Individual movies were 100 s long (3000 frames) and included an average of 500 trajectories or more. The spatial resolution of the entire setup is 0.118 μm per pixel for a 100× objective. For all sample solutions, the measured MSD data were found to grow linearly with τ (see an example plot in Scheme 1). The slope of MSD vs. τ then gave the diffusion coefficient of the probe particles. To minimize errors due to sample preparation as well as to ensure

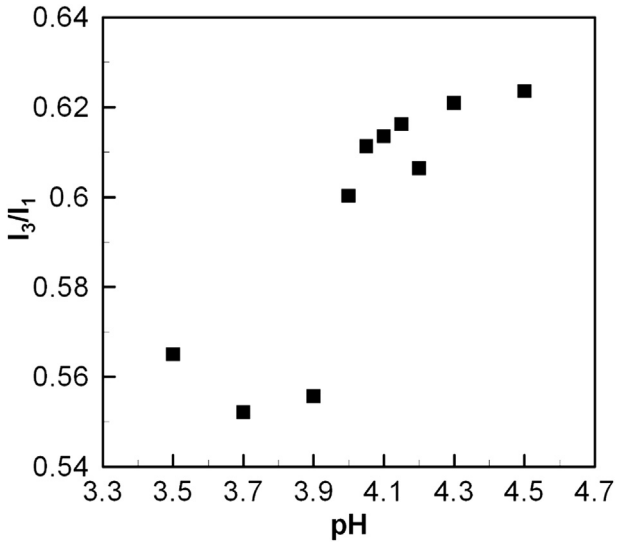

Fig. 5. Plot of pyrene emission ratio I_3/I_1 against pH for **2-VP2400** solution, where I_3 and I_1 stand for the respective intensities at emission wavelengths 372 nm and 385 nm. The sharp rise indicates a significant increase in the chain's hydrophobicity. Note that the transition point pH $\approx$ 4 is close to the transition point pH $\approx$ 4.1 seen in Fig. 2, suggesting that hydrophobic attraction between chain segments must be involved in the observed chain shrinkage phenomenon. The monomer concentrations used at pH $\leqq$ 4.1 and pH $>$ 4.1 were 0.0014 and 0.02 M, respectively. Here because pyrene emission typically has a very short lifetime, for given a sample we only scanned the spectra once to measure their intensities instantly without significant decay. For the same solution but prepared by different batches, the measured ratio could shift due to a change of the baseline. Nevertheless, the trend basically does not change qualitatively. So we use this plot as a representative figure to highlight the effects.

the statistics, for each sample we also repeated the measurement multiple times. To further validate this PTμR approach for measuring viscosity, the data were compared to those obtained by independent viscosity measurements using the Ostwald glass capillary viscometers (Schott, Germany). The validation was made specifically by measuring how the solution viscosity η varies as a function of C_m and by comparing the data using these two methods.

For dilute polymer solutions, it is well known that η grows linearly with C_m. That is, the intrinsic viscosity $[\eta]$ does not change with C_m. In contrast, in the semidilute regime, such independence of $[\eta]$ on C_m will be lost. In the experiment, we monitored the profile of $[\eta]$ by gradually increasing C_m from low to high values. When $[\eta]$ started to change with C_m, we took the turning point to be C_m^*. Notice that C_m^* can vary with molecular weight M_w. According to the classical Flory–de Gennes theory, C_m^* varies with the chain size as $N/R^3 \propto N^{1-3\nu}$ and hence as $M_w^{-\gamma}$, where $\gamma \equiv 3\nu - 1 = 0.8$ and 0 for good solvents ($\nu = 3/5$) and poor solvents ($\nu = 1/3$), respectively. Once C_m^* is determined for a certain M_w, those for other values of M_w can be immediately known. But in order to more accurately determine both the coil and globule sizes of a P2VP chain, one needs C_m to be sufficiently large for rendering discernable changes in solution viscosity. Knowing C_m^* would provide useful guidance for choosing proper values of C_m for determining these sizes from the viscosity data. For instance, if one takes C_m below C_m^* for a given molecular weight, say, M_{w1}, the same or smaller concentration can be used for solutions with M_w smaller than M_{w1} because $C_m < C_m^*(M_{w1}) < C_m^*(M_w)$.

3.4. Small angle X-ray scattering (SAXS)

We also performed SAXS to see how P2VP changes its shape and structure for complementing the PTμR data with more detailed structural information. The SAXS measurements were performed using a SAXSess mc2 system (Anton Paar KG, Austria) equipped with a sealed tube microsource and a line collimator, operated at 40 kV and 50 mA, producing Cu Kα radiation having a wavelength of 0.154 nm. Data treatment was done using SAXSquant 3.5 (Anton Paar, Austria) and Igor Pro (Wavemetrics) software packages. The background subtracted data were desmeared against the beam length profile of the source. Samples were measured in a 1 mm quartz capillary at 25 °C. Data also were collected using the 23A SWAXS endstation of the National Synchrotron Radiation Research Center [34]. With a beam of 10.0 keV (wavelength $\lambda = 0.124$ nm) and a sample-to-detector distance of 2830 mm, SAXS data were collected using a pixel detector Pilatus-1MF of an active area of 169 $\times$ 179 mm^2 and a detector pixel resolution of 172 μm. The scattering wavevector $q = 4\pi\lambda^{-1}\sin\theta$, defined by the scattering angle θ and λ, was calibrated with a standard sample of silver behenate. SAXS data were subtracted with the scattering from the same salt solutions without the polymers, and corrected for

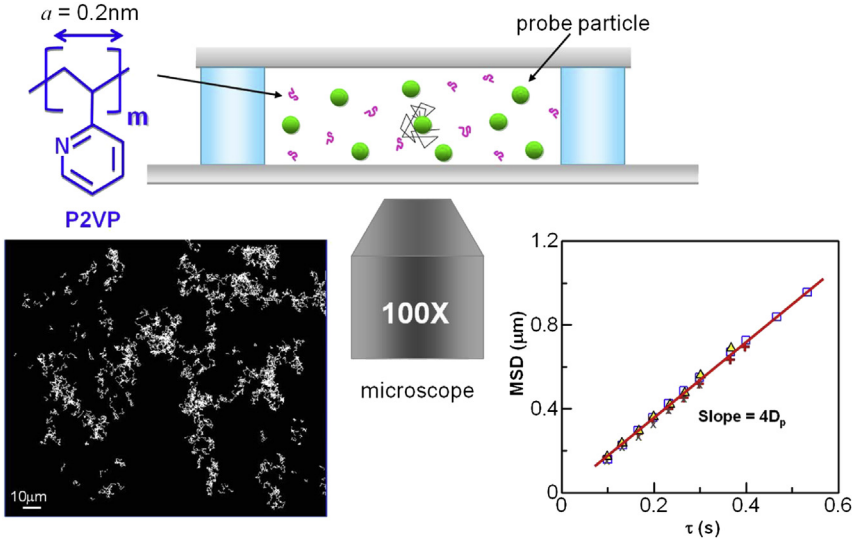

Scheme 1. Schematic illustration of particle tracking experiment for measuring viscosity of a P2VP solution. The experiment is conduced in a sealed PDMS microdevice (18 mm $\times$ 10 mm $\times$ 190 μm) on a glass substrate under an inverted microscope.

incoming flux, sample thickness and electronic noise of the detector, as detailed in a previous report [34].

3.5. Pyrene emission spectroscopy

To see whether and how hydrophobic effects play roles in the conformational changes of P2VP, the standard pyrene probing was employed to evaluate the extent of the hydrophobicity of P2VP. 20 μL of pyrene solution (1.0×10^{-5} M) in acetone was added into a glass vial and the solvent was evaporated under nitrogen gas stream. 2 mL of P2VP solution at a given pH value was added into the vial and the mixture sat still for 20 h. Pyrene emission spectra were recorded every 1 s in the wavelength range 350–500 nm using a fluorescence spectrophotometer (Hitachi FL-4500, Japan). The above procedures were repeated for P2VP solutions at different pH values. Here because pyrene emission typically has a very short lifetime, for given a sample we only scanned the spectra once and measured their intensities instantly without significant decay. We also noticed that even for the same solution but prepared by different batches, the measured ratio could shift due to a change of the baseline, sensitive to sample preparation and environment. To avoid this problem, all the data points (in which each was only measured once) were taken from the samples prepared by the same batch. By comparing the intensity (I_{372}) at 372 nm to that (I_{385}) at 385 nm for a range of pH, the greater their ratio I_{372}/I_{385} would indicate the more hydrophobic the chain would become.

4. Results and discussion

4.1. Determination of C_m^* by PTμR

Prior to studying conformational transition of P2VP using PTμR, we first validate the use of PTμR for measuring solution viscosity as well as to determine C_m^*. Fig. 1 plots $[\eta]$ against C_m for **2-VP1500**, with pH being taken far below or beyond the CGT point pH ≈ 4 [9]. For both cases, the data using PTμR, within experimental errors, basically agree with those measured by the Ostwald viscometer. The respective C_m^* values for pH < 4 and pH > 4 are about 0.003 and 0.06 M, which seem insensitive to the actual pH value in the corresponding pH regime. For other molecular weights, C_m^* can be estimated using the Flory–de Gennes theory (see Section 3.3) as follows. For pH < 4, we expect the chains to behave like swollen coils. So we use $C_m^* \propto M_w^{-0.8}$ to estimate C_m^* for **2-VP70**, **2-VP350**, and **2-VP2400** as 0.035, 0.0096, 0.0021 M, respectively. As for pH > 4 where we expect the chains to turn into the more compact globular state, since C_m^* is independent of M_w, it is always 0.06 M regardless the chain length. We should point out that in obtaining the above C_m^* values, we make an *a prior* assumption that P2VP for pH < 4 and pH > 4 follows the coil and globule scalings predicted by the Flory–de Gennes theory (see Section 3.3). The consistency concerning whether the solutions are sufficiently dilute to capture the conformational change of P2VP will be verified *a posteriori* in Section 4.3.

4.2. Conformational changes of P2VP probed by PTμR

Having determined C_m^*, we selected suitable monomer concentrations below the overlap values for both swollen and compact states to measure the intrinsic viscosity $[\eta]$ and hence the hydrodynamic radius R_h of P2VP. It is worth noting that the volume fractions of P2VP coils and globules used for measurements were well below 15%. Fig. 2 plots the calculated hydrodynamic radius (R_h) against pH for solutions **2-VP350** (degree of polymerization, DP = 350) and **2-VP1500** (DP = 1500). At first glance, the data, together with the corresponding $[\eta]$ (see the inset), display significant drops around pH = 4.1, implying an occurrence of chain collapse. But taking a more close look at the figure, we find that the detailed transition behavior seems to be molecular-weight dependent. For **2-VP1500**, the transition is found quite abrupt, as R_h decreases very sharply from 28.0 nm to 11.3 nm. For **2-VP350**, however, the transition appears less dramatic with R_h changing from 13.2 nm to 6.6 nm. Compared to **2-VP1500**, the transition point for this case also seems to shift toward a slightly higher pH value. These observations basically agree with those seen in previous reports using FCS [9,10]. The above results also confirm the well-known chain-size dependent feature of coil–globule transition shown by de Gennes [2]—the transition is relatively smooth for short chains, but turns jump-like for sufficiently long chains, akin to the common first-order phase transitions resulted by taking the infinite size limit (i.e. the thermodynamic limit) [35].

Wang and Zhao [9] reported in their FCS study that the coil and globule sizes for P2VP of M_w = 109,800 g/mol (DP = 1000) in a salt-free solution were 22.6 nm and 6.8 nm, respectively. Here we take our data at M_w = 159,000 g/mol (**2-VP1500**) to compare with 28.2 nm and 7.7 nm found by interpolating their data using R (coil) ~ $M_w^{3/5}$ and R (globule) ~ $M_w^{1/3}$. In our study, the coil size is 28.0 nm, in very good agreement with 28.2 nm estimated from the FCS data. However, our globule size 11.3 nm is slightly larger than that 7.7 nm from the FCS data. This slight discrepancy can be attributed to the fact that the conformations of P2VP with added salts in our study are actually different from those without salts in the FCS study by Wang and Zhao [9], which will be discussed in more detail in Section 4.6.

4.3. Scaling of hydrodynamic radius vs. molecular weight

We have validated PTμR for measuring solution viscosity and demonstrated its use in revealing the abrupt reduction in the chain size of P2VP due to pH effects. While this size reduction does imply chain shrinkage, it can only be formally claimed if the two conformational states – swollen coil and compact globule – are identified. This can be achieved by measuring how the chain sizes vary with M_w below and beyond the transition point. According to the classical Flory–de Gennes theory, the chain sizes at the coiled and globular states scale as R (coil) ~ $M_w^{3/5}$ and R (globule) ~ $M_w^{1/3}$, respectively. If the R_h values follow the above scalings, the use of PTμR for probing CGT can then be justified.

Fig. 3 shows the calculated R_h against M_w, showing distinct power laws for pH = 3.9 and pH = 4.3 with the correlation coefficient 0.99. Moreover, the fitted exponents for pH = 3.9 and pH = 4.3 are found to be 0.592 ± 0.006 and 0.339 ± 0.010, respectively, in excellent agreement with $M_w^{0.6}$ and $M_w^{0.33}$ predicted by the classical Flory–de Gennes theory. This also confirms that P2VP for pH < 4.1 indeed behaves like a swollen coil and shrinks to a compact globule for pH > 4.1. In fact, the swelling exponent at the coiled state shows a much better agreement with 0.588 obtained by the renormalization group theory [36].

A previous FCS study by Wang and Zhu [10] also measured the dependence of R_h on M_w, and found R (coil) ~ $M_w^{0.67}$ and R (globule) ~ $M_w^{0.35}$. The swelling exponent in the former is larger than ours. Notice that their experiments were conducted in water without added salts. So their P2VP chains at low pH might somewhat resemble highly charged polyelectrolytes in poor solvents. Owing to strong electrostatic repulsions between chain segments, it has been reported theoretically as well as experimentally that such P2VP chains could look more extended or even take necklace-like structures [12,37,38]. A possible existence of more extended chains might explain the slightly greater swelling exponent found in their study. But such chain conformations would unlikely exist in the present study where the amount of salts is excessively high, this

explains why the swelling exponent in our study gives a much better match with the well known value 0.588 predicted by the renormalization theory [36].

In contrast to the FCS study by Wang and Zhu [10], we have added plentiful salts (1 M NaCl) in our P2VP solutions. As this would produce much stronger screening on chain charges to greatly diminish electrostatic repulsion between chain segments, the chains would become less extended and hence more likely take the coiled form. In fact, at sufficiently high salt concentrations, polyelectrolytes actually behave like neutral polymer chains [39]. It is this reason why the swelling exponent found in our study shows much better agreement with the theory than Wang and Zhu's [10]. The possible existence of more extended P2VP chains in their study might also explain why the observed conformational transition is less abrupt than ours. A more in-depth theoretical analysis about how P2VP changes its conformation will be discussed in Section 4.6.

4.4. SAXS study on conformational transition of P2VP

To gain more insights into how P2VP changes its size and structure, SAXS experiments are also carried out. Fig. 4a and b shows the SAXS intensity profiles against the scattering vector q for **2-VP70** at pH = 3.7 and pH = 4.5 below and above the transition point pH ≈ 4.1. The data for each case have been subtracted from the background 1 M NaCl solution at the corresponding pH value. As shown in Fig. 4a, the data at both the pH values show steep upturns in the low q regime for $q < 0.02$ Å^{-1}. Given that we have subtracted the intensity from the background scattering from free salt ions, we suspect that these upturns could come from Na^+ absorbed on polymer chains or possible formation of ionomers [40]. Perhaps the signature of ionomers can be best indicated by the upturn at pH = 3.7, showing $q^{-3.8}$ decay close to q^{-4} based on the Debye–Bueche model [41]. But looking at the high q regime such as $q > 0.02$ Å^{-1}, completely different characteristics are revealed: the pH = 3.7 plot shows a long tail with much slower decay while a more rapid decline is observed for pH = 4.5, implying that the chain must undergo a significant conformation change. At pH = 3.7, we expect that the chain looks like a swollen coil with $R_h \sim M_w^{0.6}$. But perhaps because of being outshined by the strong upturn, the scattering spectrum here neither displays any Guinier-like plateau in the low q regime nor shows the fractal signature $q^{-1/\nu} = q^{-1.7}$ in the high q regime. While it seems conceivable that the more extended chains here could be attributed to electrostatic repulsion between chain segments, the distinctive peak associated with the Debye correlation is actually suppressed by abundant salt ions in 1 M NaCl solution we used here. Nevertheless, as the present chain conformational change involves the association/dissociation of H^+ ions, the participation of charge effects in intrachain interactions is evident.

At pH = 4.5, we expect that the chain shrinks to a compact globule. Since the more compact chain structure has a greater scattering reflectivity, its structural information might be better revealed with less influence by the upturn. Indeed, not only the upturn becomes less steep, but also the much more apparent hard sphere signature Porod law q^{-4} is revealed for $q > 0.02$ Å^{-1}. The former implies that the chain segments are less correlated, and the latter seems to indicate close packing of these segments. These results strongly imply that the chain collapses into a dense and isotropic globule without internal structures. The fitted globule size using the hard sphere model is $R_h \approx 5.7 \pm 1.7$ nm, in reasonable agreement with the calculated value using PTμR (see Fig. 3). In addition, we observe that the rapid q^{-4} decay seems to approach asymptotically toward $q = 0.1$ Å^{-1}. This particular q can be thought of as the first zero of the periodic hard sphere spectrum. Its length $2\pi/q \sim 6$ nm actually provides a good estimate for the globule size, which is close to the fitted value given above.

Fig. 4c shows the SAXS spectra for larger molecular weight **2-VP1500** solutions. In this case, because the density of the chain segments is much lower than that of **2-VP70** (since $\rho \sim N/R^3$ decays like $N^{-(3\nu-1)}$ with $\nu \geq 1/3$), the scattering signatures seem dominated by the upturns and hence become less apparent. Nevertheless, the following features still imply a conformational transition. At pH = 3.7, the data curve basically looks similar to that of **2-VP70** (Fig. 4b). At pH = 4.5, the slope of the upturn in the low q regime is smaller than that at pH = 3.7. In addition, we observe a small hump for $q = 0.02$–0.1 Å^{-1}, a little downward cusp at around $q = 0.1$ Å^{-1} followed by another hump for $q > 0.1$ Å^{-1}. These features seem to resemble the periodic humps seen in the hard-sphere spectrum, which again implies a more compact structure for the chain.

4.5. Pyrene spectroscopy for studying effects of pH on hydrophobicity of P2VP

Fig. 5 plots the measured pyrene emission ratio I_{372}/I_{385} against pH for **2-VP2400**. Here we choose **2-VP2400** because it is the longest chain among our P2VP samples and expected to have the greatest pyrene emission intensity. The result reveals a sharp increase from 0.56 to 0.62 at pH ≈ 4 when pH changes from 3.5 to 4.5, indicating a significant rise in the chain's hydrophobicity. In addition, the transition point pH ≈ 4 is fairly close to the transition point pH ≈ 4.1 seen in Fig. 2, implying that the observed conformational transition might be triggered by this hydrophobicity change.

Perhaps the observed rise in the chain's hydrophobicity can be interpreted as a consequence of diminished water contacts due to fewer hydration shells around P2VP when it becomes less protonated. If the chain's hydrophobicity can be roughly represented by the number of deprotonated chain segments, we can use the acid dissociation constant pK_a to estimate the degree of protonation and hence the chain's hydrophobicity. Taking $pK_a \approx 4.5$ for P2VP [42], we can estimate that at the transition point pH ≈ 4, there are about 25% of chain segments being deprotonated. Changing pH to a smaller value pH = 3.9 results in 20% of deprotonation, whilst a slightly higher pH = 4.1 gives 28%. So compared to pH = 4, the relative changes of the chain's hydrophobicity for pH = 3.9 and pH = 4.1 are 20% and 12%, respectively, in rough agreement with what we see in Fig. 5. Given that less than 30% of chain segments are deprotonated and that not more than 20% of them can trigger the transition, the impacts on chain collapse due to the chain's hydrophobicity changes are quite remarkable. It is also clear that the more hydrophobic chain segments, the more inclined for them to clump together by minimizing their contacts with the surrounding solvent. Also because intersegment electrostatic repulsion is largely screened by added salts, this hydrophobic intrachain attraction provides a natural explanation why P2VP chains at pH > 4 must collapse into compact globules, thereby showing the distinctive hard-sphere signature in accordance with the 1/3 swelling exponent and the Porod-type SAXS spectrum seen earlier.

At pH < 4 the chain's hydrophobicity become diminished. But we have demonstrated in Fig. 3 that the chains in this case actually behave like swollen coils. This implies that interactions between chain segments are dominated by repulsion and this repulsion has to be stronger than the attraction caused by the chain's hydrophobicity. As the observed chain shrinkage is triggered by pH change and sensitive to the degree of protonation, such intrachain repulsion can only be attributed to the charges along the P2VP backbone. So whether a P2VP chain expands or collapses would be determined by if it is electrostatic (or excluded volume) repulsion or hydrophobic attraction dominating intrachain interactions. In

general, for a charged polymer chain like P2VP, it can exhibit a variety of conformational states due to interplays between these two effects. As will be discussed below, it actually turns out that P2VP, because of strong charge screening by added salts, would behave like a neutral polymer chain, allowing us to describe its conformational transition under the usual Flory–de Gennes framework.

4.6. Mechanism of the observed coil–globule transition

In this section we would like to provide more in-depth insights into the pH-induced coil–globule transition phenomenon of P2VP. While we have validated the use of microrheology in probing such a transition and showed excellent agreement with the predictions by the Flory–de Gennes theory, this theory does not specifically take pH effects into account. This section is to fill up this gap. In addition, we want to see how P2VP changes its conformation due to pH effects, especially with added salts, in terms of intersegment interactions in connection to experimental observations.

The observed conformational transition phenomenon for P2VP appears to be one among many conformational transitions of weakly charged polyelectrolyte chains seen in previous reports [9]. Polyelectrolytes can be either quenched (with fixed chain bare charges), or annealed (with varying chain bare charges) like P2VP whose charges depend on the degree of protonation. In either case, the nature of conformational transitions is quite subtle, strongly depending on how electrostatic intrachain interactions interplay with solvent quality effects closely related to the hydrophobicity of a chain. Also because electrostatic intrachain interactions depend on the net charge of a chain and on the ability of ionic species to screen the chain charge, whether salts exist or not plays vital roles in chain conformations.

When there are no added salts, the charge screening comes solely from a chain's own countercharge (which is H^+ for P2VP). In this case, the chain in a good solvent would take the elongated form [39]. But in a poor solvent, such an elongated chain could tend to collapse into a small globule. However, such a charged globule, just like a charged droplet, is not always thermodynamically stable [43]. If the chain charge were high, the electrostatic energy of the globule would be prohibitively high. In order to lower its energy, the globule would tend to spilt into a number of smaller beads, undergoing the so-called *pearl-necklace* transition [38].

Our study differs from the above in that we have added a plenty of salts into P2VP solutions. Since there are much more counterions supplied from the salty background having a much higher ionic strength, they are able to screen most of the chain charges along the P2VP backbone. Since charge screening is merely effective within thin Debye layers around a P2VP chain, the chain, in a far distance view, would look like a neutral polymer chain [39]. This explains why P2VP chains here have to take the spherical form and why the calculated hydrodynamic radii show perfect agreement with the Flory–de Gennes theory.

Scheme 2 sketches the plausible mechanism responsible for the observed coil–globule transition due to pH changes. At low pH, P2VP is highly protonated so that intersegment interactions are dominated by electrostatic or excluded volume repulsion (or both), which tends to swell the chain. At high pH, however, the chain becomes less protonated, weakening the ability to uptake water molecules into the chain. Because the chain backbone is essentially hydrophobic, the tendency to minimize its contacts with the surrounding water molecules would collapse the chain, making chain segments look as if they attract to each other.

In line with the above, to get more quantitative insights into how P2VP expands or collapses, it is more convenient to look at the

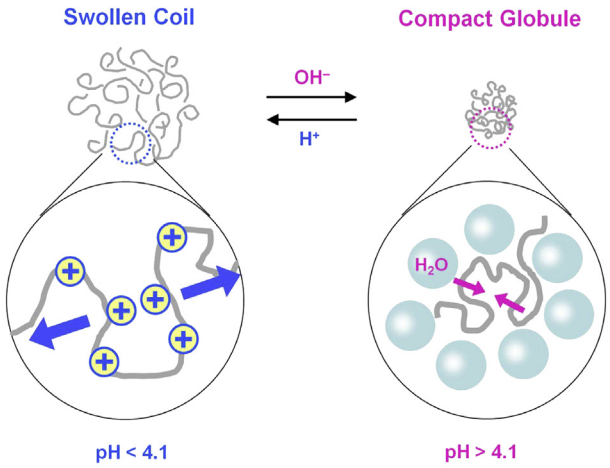

Scheme 2. Schematic mechanism of pH-induced coil–globule transition for P2VP. At pH below the transition point pH ≈ 4.1, intersegment interactions are dominated by electrostatic or excluded volume repulsion, which tends to swell the chain. At pH greater than the transition point, hydrophobic attraction between chain segments tends to collapse the chain into a compact globule.

chain free energy landscape Eq. (1) in terms of the swelling factor α b$R/bN^{1/2}$ according to de Gennes [2]:

$$\frac{F}{k_BT} = 3\left(\frac{1}{2}\alpha^2 - \ln\alpha\right) + \frac{B}{\alpha^3} + \frac{C}{\alpha^6}, \tag{7}$$

where $B = (v_2/b^3)N^{1/2}$ and $C = v_3/b^6$ denote the dimensionless 2nd and 3rd virial coefficients, respectively. Minimization of Eq. (7) with respect to α determines coil/globule size of a polymer chain:

$$\alpha^5 - \alpha^3 + \frac{2C}{\alpha^3} = B, \tag{8}$$

It has been shown by de Gennes [2] that Eq. (8) can admit multiple solutions when B is slightly negative and C (>0) is sufficiently small.

To see more clearly how such multiplicity is related to conformational transition, we plot how α changes with B and C in Fig. 6a. The result clearly reveals two distinct states: one is $\alpha > 1$ corresponding to the coiled state with $B > 0$, and the other is $\alpha < 1$ corresponding to the globular state with $B < 0$. But when C is decreased to 0.01 or smaller, multiple solutions can exist for $-0.2 < B < 0$. As also seen in Fig. 6b, this case corresponds to the situation where the chain's energy landscape exhibits two minima and an unstable maximum in between. Similar to vapor–liquid phase transition, this multi-solution situation must lead to a jump like phase transition for ensuring equal chemical potentials at both the coiled and globular states (i.e. the Maxwell equal area rule) and thereby the coexistence of these two states. Note that this sharp conformational transition cannot be captured without the α^3 term in Eq. (8) (from the ln α term in Eq. (7)). As this term guarantees the ideal state $\alpha = 1$ at $B = 0$ over which a polymer chain at the higher energy coiled state must pass before moving to the lower energy globule state, this explains why the energy landscape exhibits two minima and a maximum near the transition point.

It is also worth mentioning that the energy at the globular state is $F_{globule}/k_BT \sim -B^2/C = -(v_2^2/v_3)N$. To see an apparent transition, this energy must be at least an order of the thermal energy k_BT, giving $B^2/C \sim O(1)$. As this transition can only occur near the theta point within a window like $|B| \sim 10^{-1}$, one needs $C \sim 10^{-2}$ according to the above criterion. This also explains why an abrupt transition can only occur with such values of B and C, as shown by

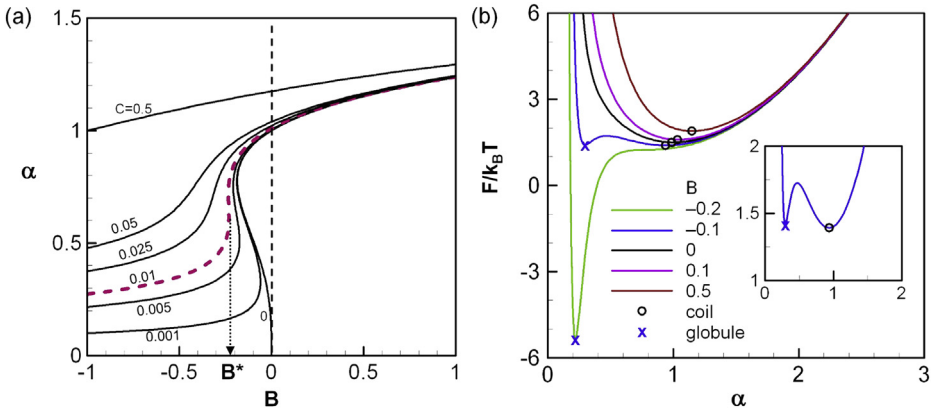

Fig. 6. (a) Plot of the swelling factor α against the dimensionless 2nd virial coefficient B for various values of the dimensionless 3rd virial coefficient C. It clearly reveals that multiple solutions can exist for $B < B^* \approx 0.2$ and $C < 0.01$. Similar to vapor–liquid phase transition, this multiplicity leads to a co-existence between the coiled state ($\alpha > 1$) and the globular state ($\alpha < 1$), suggesting a jump-like transition near the transition point B^*. (b) Shows how the free energy F/k_BT varies with α for various values of B at $C = 0.001$. As B decreases from a positive value to a negative one, the free energy minimum shifts from a larger α (>1) to a smaller value (<1), indicating a transition from the coiled state to the globular state. At $B = -0.1$, in particular, there exist two stable minima and an unstable maximum, corresponding to multiple solutions seen in (a).

de Gennes [2] as well as in Fig. 6a. In terms of $\tau = |v2|/v_3^{1/2}$ that measures the width of the transition near the theta point, $B^2/C \sim O(1)$ also leads to

$$\tau \sim N^{-1/2} \tag{9}$$

It thus follows that the longer a chain, the smaller τ and hence the sharper the transition. This explains why sharp chain shrinkage is often observed for long chains, as seen in Fig. 2 as well as in most experiments.

In terms of the present pH-induced coil–globule transition, pH can affect both v_2 and v_3 in the following ways. For the second virial coefficient v_2, it consists of three parts:

$$v_2 = v_2^{\text{bare}} + v_2^{\text{el}} + v_2^{\text{pH}} \tag{10}$$

where $v_2^{\text{bare}} \sim b^3$ measures the excluded volume of bare chain segments (due mostly to the aromatic ring of P2VP), $v_2^{\text{el}} \sim \ell_B \lambda^2 f^2$ (with $\ell_B = 0.7$ nm the Bjerrum length, λ the Debye screening length, and f the fraction of charged segments) accounts for electrostatic repulsion according to the Odijk–Skolnick–Fixman theory for flexible polyelectrolytes with added salts [44,45], and $v_2^{\text{pH}} (< 0)$ reflects hydrophobic attraction that is only important when chain segments become less protonated (beyond the transition point pH $\approx$ 4.1). With $b \approx 1.8$ nm (which is assumed to be polystyrene's [46]), $f \approx 0.3$, and $\lambda \approx 0.3$ nm, we find $v_2^{\text{bare}} \sim 5.83$ nm^3 and $v_2^{\text{el}} \sim 0.006$ nm^3, indicating that excluded volume dominates over electrostatic repulsion. Given that P2VP chains are actually charged due to protonation, rather weak electrostatic repulsion here can only be attributed to strong charge screening by added salts. This is the reason why P2VP in a very salty background looks like a neutral polymer chain and hence its behavior can be well described by the classical Flory–de Gennes theory. Also because of this strong screening by salt ions, v_2^{el} does not change significantly with pH. So for pH below the transition point pH $\approx$ 4.1, the total excluded volume is $v_2^{\text{total}} \sim 5.84$ nm^3, giving the effective persistence length $\ell_{\text{eff}} \sim v_2^{\text{total}}/b^2 \sim 1.8$ nm not much different from b. Therefore, to see chain collapse by turning the intrachain interactions to be attractive, v_2^{pH} has to be more negative than -5.84 nm^3.

In terms of chain rigidity, it might also be sensitive to pH because the lack of hydration shells beyond the transition point would make ℓ_{eff} smaller than that below the point. In other words, a less protonated P2VP chain beyond the transition point would be more flexible than a more protonated one below the point, making the former more compressible than the latter and thereby causing a change in the third virial coefficient v_3 before and after the transition point. At the less protonated state with pH > 4.1, v_3 would scale like $[\ell_{\text{eff}}(\text{pH} > 4.1)]^6$ and hence become significantly smaller than that at the more protonated state with pH < 4.1. If taking $C = [v_3/\ell_{\text{eff}}(\text{pH} < 4.1)]^6 \sim [\ell_{\text{eff}}(\text{pH} > 4.1)/\ell_{\text{eff}}(\text{pH} < 4.1)]^6 \sim 0.01$ with respect to the more protonated state, one would need to have $\ell_{\text{eff}}(\text{pH} > 4.1)$ reduced to about 50% of $\ell_{\text{eff}}(\text{pH} < 4.1)$ to see an abrupt chain collapse.

5. Concluding remarks

We have validated the use of PTμR in determining how P2VP changes its hydrodynamic radius due to pH changes, thereby enabling to quantify its coil–globule transition. To our best knowledge, this is the first quantitative demonstration that PTμR can be applied to probe the conformational transition of a polymer chain. We not only observe the sharp coil–globule transition near pH = 4 seen by previous reports, but also show that the calculated swelling exponents are in excellent agreement with those predicted by the classical Flory–de Gennes theory. We also carry out SAXS and pyrene studies to gain more insights into this pH-induced conformational transition phenomenon. The SAXS spectra at the less protonated state for pH > 4 display the distinctive Porod-type decay, indicating a more compact, hard-sphere-like internal structure within a P2VP chain. This observation is consistent with chain collapse by much stronger chain's hydrophobicity for pH > 4, signified by the sharp rise seen in the pyrene spectrum. We further identify that the observed coil–globule transition is determined by interplays between excluded volume repulsion, electrostatic repulsion, and hydrophobic attraction at the subunit level of a P2VP chain, sensitive to the degree of protonation near the transition point. This new application of PTμR not only offers a simple and reliable mean for revealing microstructures of polymer chains, but also has potential uses in exploring the physics of polymer systems at the nano/molecular scales.

Acknowledgments

This work is supported by the Ministry of Science and Technology of Taiwan under grant no. 01-2221-E-006-230-MY3 of HHW.

References

[1] Nishio I, Sun S-T, Swislow G, Tanaka T. Nature 1979;281:208–9.
[2] de Gennes P-G. J Phys Lett 1975;36:55–7.
[3] Wu C, Zhou S. Macromolecules 1995;28:8381–7.
[4] Dusek K, Patterson D. J Polym Sci B Polym Phys Ed 1968;6:1209–16.
[5] Bloomfield VA. Biopolymers 1997;44:269–82.
[6] Teif VB, Bohinc K. Prog Biophys Mol Biol 2011;105:208–22.
[7] Scheutjens JMHM, Fleer GJ. J Phys Chem 1979;83:1619–35.
[8] Heineck ME, Cardoso MB, Giacomelli FC, da Silveria NP. Polymer 2008;49:4386–92.
[9] Wang S, Zhao J. J Chem Phys 2007;126:091104.
[10] Wang S, Zhu Y. Soft Matter 2011;7:7410–5.
[11] Kirwan LJ, Papastavrou G, Borkovec M. Nano Lett 2004;4:149–52.
[12] Minko S, Kiriy A, Gorodyska G, Stamm M. J Am Chem Soc 2002;124:3218–9.
[13] Liu W, Liu Y, Zeng G, Liu R, Huang Y. Polymer 2012;53:1005–14.
[14] Lee H, Boyce JR, Nese A, Sheiko SS, Matyjaszewski K. Polymer 2008;49:5490–6.
[15] Aseyev VO, Klenin SI, Tenhu H, Grillo I, Geissler E. Macromolecules 2001;34:3706–9.
[16] Nishi K, Hiroi T, Hashimoto K, Fujii K, Han Y-S, Kim T-H, et al. Macromolecules 2013;46:6225–32.
[17] Tam KC, Wu XY, Pelton RH. Polymer 1992;33:436–8.
[18] Yang H, Cheng R, Wang Z. Polymer 2003;44:7175–80.
[19] Crocker JC, Grier CG. J Colloid Interface Sci 1996;179:298–310.
[20] Squires TM, Mason TG. Annu Rev Fluid Mech 2010;42:413–38.
[21] MacKintosh FC, Schmidt CF. Curr Opin Colloid Interface Sci 1999;4:300–7.
[22] Breedveld V, Pine DJ. J Mater Sci 2003;38:4461–70.
[23] Tu RS, Breedveld V. Phys Rev E 2005;72:041914.
[24] Jan J-S, Breedveld V. Macromolecules 2008;41:6517–22.
[25] Hsiao PY, Luijten E. Phys Rev Lett 2006;97:148301.
[26] Ortega F, Ritacco H, Rubio RG. Curr Opin Colloid Interface Sci 2010;15:237–45.
[27] Dasgupta BR, Weitz DA. Phys Rev E 2005;71:21504.
[28] Cicuta P, Donald AM. Soft Matter 2007;3:1449–55.
[29] Kohli I, Mukhopadhyay A. Macromolecules 2012;45:6143–9.
[30] Chapman CD, Lee K, Henze D, Smith DE, Robertson-Anderson RM. Macromolecules 2014;47:1181–6.
[31] Sarmiento-Gomez E, Santamaria-Holek I, Castillo R. J Phys Chem B 2014;118:1146–58.
[32] Einstein A. Investigations on the theory of Brownian movement. New York: Dover; 1956.
[33] Batchelor GK. J Fluid Mech 1977;83:97–117.
[34] Jeng U, Su CH, Su C-J, Liao K-F, Chuang W-T, Lai Y-H, et al. J Appl Cryst 2010;43:110–21.
[35] Stanley HE. Introduction to phase transitions and critical phenomena. New York: Oxford University Press; 1971.
[36] Le Guillou JC, Zinn-Justin J. Phys Rev Lett 1977;39:95–8.
[37] Raphael E, Joanny J-F. Europhys Lett 1990;13:623–8.
[38] Dobrynin AV, Rubinstein M, Obukhov SP. Macromolecules 1996;29:2974–9.
[39] Dorbrynin AV, Colby R, Rubinstein M. Macromolecules 1995;28:1859–71.
[40] Wu DQ, Phillips JC, Lundberg RD, Macknight WJ, Chu B. Macromolecules 1989;22:992–5.
[41] Debye P, Bueche AM. J Appl Phys 1949;20:518–25.
[42] Tantavichet N, Pritzker MD, Burns CM. J Appl Polym Sci 2001;81:1493–7.
[43] Rayleigh L. Philos Mag 1882;14:184–6.
[44] Odijk T. J Polym Sci B Polym Phys Ed 1977;15:477–83.
[45] Skolnick J, Fixman M. Macromolecules 1977;10:944–8.
[46] Rubinstein M, Colby R. Polymer physics. New York: Oxford University Press; 2003.